

Island photonic structures: Properties and application in sensing and metrology

E.Ya. Glushko^{1*}, A.N. Stepanyuk²

¹*V. Lashkaryov Institute of Semiconductor Physics, NAS of Ukraine
45, prospect Nauky, 03680 Kyiv, Ukraine,*

²*Krivyi Rih State Pedagogical University,
54, prospect Gagarina, 50086 Krivyi Rih, Ukraine*

*Corresponding author: scientist.com_eugene.glushko@mail.com

Abstract. In this work, we consider a novel photonic crystal type, island resonator, perspective objects of all-optical processing domain, which can be used in the logic gate and adder architecture. Another kind of novel structures, gas-containing pneumatic photonic crystal, was considered as an optical indicator of pressure uniting several pressure scales of magnitude. This type of device includes layered elastic platform, optical fibers and switching valves, all enclosed into a chamber. We have investigated theoretically distribution of deformation and pressure inside a pneumatic photonic crystal, its bandgap structure and light reflection changes depending on the influence of external pressure and temperature. A method has been proposed to determine the fundamental molar gas constant R with the relative standard uncertainty near 10^{-10} that is based on extra accurate volume controlling and high sensitive pressure measurements in the framework of scale echeloning procedure.

Keywords: pneumatic photonic resonator, optical devices, biosensors, precise pressure measurement, molar gas constant.

<https://doi.org/10.15407/spqeo22.04.430>

PACS 06.20.Dk, 07.07.Df, 42.70.-a, 43.20.Ks

Manuscript received 13.04.19; revised version received 06.05.19; accepted for publication 29.10.19; published online 08.11.19.

1. Introduction

A significant challenge faced by the modern civilization is to resolve the existing global problems of ecology, human survival, economical development, scientific investigations and many others, which demand extra high computer power [1]. The awaited expansion from the today existing petaflop computer stations to the exaflop capable machines may be intensified using new paradigms both for the element base and design of computers, in particular those like quantum and optical. Among the advantages of all-optical principles use in logical devices for optical computing, optical associative memories, and optical interconnections are their higher operation frequencies in signal processing, small energy losses and practically unlimited possibilities to organize parallel operating of signals. The all-optical ideology is used to mean the absence of electronic transforming of signals at any stage of the process as well as the absence of spin or phonon mechanisms in signal processing. The reason of all-optical anticipated efficiency in comparison with mixed ways is in an obvious axiom that each signal

transformation from one physical form into another one decreases the common speed of signal passage through the device. Though the outstanding optical features of photonic crystals have been first mentioned in Rayleigh study [2], a tide of the modern applications in a wide area was begun from works of Eli Yablonovitch and Sajeev John [3, 4]. Various properties of photonic structures useful to create perfect dielectric mirrors, high-performance optical filters, key elements of logic gates, controlled mirrors or flexible waveguides and for many other applications were discussed since then (see [5-9]).

At the present time, photonic crystals (PhCr) have been widely investigated as promising objects for optical technologies in computing, signal processing, telecommunication, sensorics, *etc.* [6-10]. The structure of optical spectra of photonic crystals is important for applications in optoelectronic and all-optical devices. Photonic crystals are often considered as a perfect reflecting medium surrounding the optical waveguide. Therefore, the conditions of omnidirectional gaps in photonic spectrum are of interest for determining the optimal wavelength range of optical devices [11, 12].

In Fig. 1, the today prevailing applications of photonic crystals are as follows: perfect reflectors in waveguides, signal processing, lensing and bridge-like regulators. A general criterion for complete reflection of radiation in a given frequency range for all incident angles and polarizations was formulated in [12]. In [13], an all-dielectric mirror for visible frequencies was demonstrated. Due to the used high optical contrast of the structure 10% broadening the omnidirectional range was achieved. Possible application of systems of this kind also includes creating the high-frequency waveguides for communications and power delivery. A planar circuit based on a photonic crystal designed and fabricated in silicon on silicon dioxide was considered in [14]. A two-dimensional photonic crystal served as a perfect reflector to create the total internal reflection and achieve a confinement in transversal dimension. In [15], the air-bridge type of AlGaAs photonic crystal slabs was fabricated, and the transmittance spectrum was measured. It was found that the experimentally observed TM and TE spectra are consistent with theoretically calculated band structures. It was found that for modes in the chosen frequency interval t photonic band gap takes place only for the TE-like guided modes.

If the filling factor of a 2D photonic crystal is properly tuned over the structure, a wide-band self-collimation effect can arise for optical signals [16]. The results obtained using the finite-difference time-domain simulation of the electromagnetic wave propagation through the structure has shown distinctive wide-band self-collimation of optical rays and other flat lens properties. The all-optical logic gates design based on the nonlinear elements was proposed in [17] and a partial case for the optical logic AND gate architecture was discussed in [18]. An important effect of shifting bands caused by the introduced inside PhCr $\chi^{(3)}$ -type nonlinearity was found in [19] and general features of all-optical signal processing was discussed.

In this work, we consider a novel photonic crystal type, island resonator, promising object for all-optical processing domain, which can be used in the logic gate and adder architecture. A gas-containing pneumatic photonic crystal is considered as an optical indicator of pressure uniting several pressure scales of magnitude. A procedure based on extra-accurate volume controlling and high sensitive pressure measurements is proposed to determine the universal molar gas constant R with approximately 10 significant digits accuracy.

2. Contacting photonic crystal islands

In [20], a general problem of eigenstates and eigenmodes of the island kind PhCr resonator was solved including spectrum, mode classification and modal amplitude distribution along the structure. It was found that, depending on geometry, materials and optical contrast of structures, two types of local states of electromagnetic field may exist inside a PhCr resonator besides several kinds of transmitted and waveguide standing waves. The presence of an external optically nonlinear layer covering

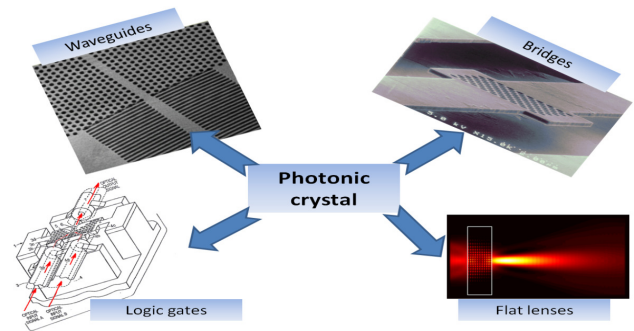


Fig. 1. Several applications of photonic crystal resonators: perfect reflectors in waveguides [13, 14], lensing and bridge-like regulators [15, 16], signal processing [17, 18].

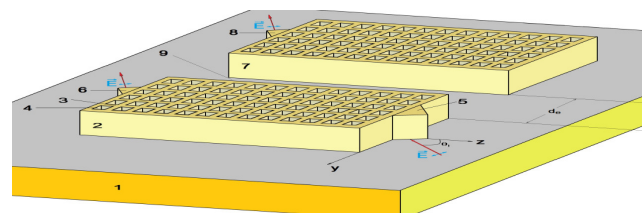


Fig. 2. Schematic of two contacting photonic crystal islands. 1 – substrate, 2 – photonic crystal *a*, 3 – matrix material, 4 – accompanying material (shown air wells), 5 – input prism of *a*-island, 6 – output prism, 7 – photonic crystal *b*, 8 – output prism of island *b*, 9 – inter-island interaction zone, θ_i – angle of incidence, p -polarized plane wave, d_c – distance between islands.

an optically linear PhCr provides an opportunity to control the beam entrance angle into the resonator due to the phenomenon of shifting bands discussed in [19]. It was shown there that the Kerr nonlinear coating layer leads to the so-called quasi-shift effect of bands inside the total internal reflection (TIR) region, causing a strong deviation in transmission and reflection of the light signal introduced into the structure through the input. It was also noted that matrix material is topologically connected whereas the system of embedded into the matrix ordered bars or wells of a concomitant material represents disconnected medium.

In Fig. 2, two oblong contacting photonic crystals containing $N_{az} \cdot N_{ay}$ and $N_{bz} \cdot N_{by}$ periods in Z - Y directions are presented. A principal topological difference between a system of infinite 1D membranes separating gaseous voids, which serves as a boundary between the left and right media whereas the mentioned case describes two photonic crystal islands in a sea of surrounding medium. The resonator's in-plane standing modes can be excited only by using an external source through the special inputs 5, 6, 8 and may be controlled due to their nonlinear properties. The photonic modes differ in terms of field density distribution inside the resonator, their dependence on frequency and geometry of incidence, which may be used in optical devices of various types.

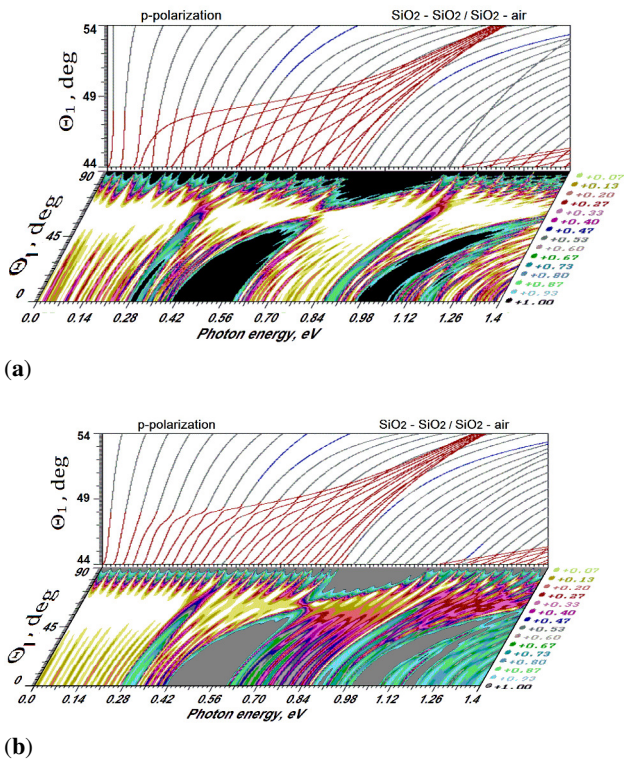


Fig. 3. TM polarized wave spectrum of two different contacting 8 period 1D PhCr. **Vertical panels** (a), (b): the bandgap structure inside the TIR region at the propagation angles θ_1 in glass from 44° to 54° . $d_{1a} = 0.5 \mu\text{m}$, $d_{2a} = 0.8 \mu\text{m}$, $d_{1b} = 0.4 \mu\text{m}$, $d_{2b} = 0.5 \mu\text{m}$, photon energy up to 1.4 eV, $\epsilon_{1a} = 3.2$, $\epsilon_{2a} = 2.3$, $\epsilon_{1b} = 3.2$, $\epsilon_{2b} = 1.0$. **Horizontal panels** (a), (b): color diagram for reflection R of the external incident beam at external (air medium) incident angles θ_1 from 0° to 90° . Right columns: color scale for reflection coefficient R_i (a). Distance between islands $d_e = 10.0 \mu\text{m}$. (b) contacted islands, $d_e = 0.2 \mu\text{m}$.

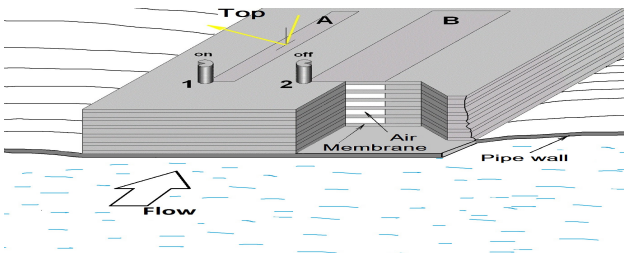


Fig. 4. A layered OPM as a multiscale pressure indicator schematically. A stack of plates contains two strip pneumatic photonic crystals A and B. 1, 2 are the switches of access to upper gaseous medium (chamber) atmosphere. Geometry of light beam incidence is shown for the strip A.

If two photonic crystals *a* and *b* are far enough one from another, then the bandgap structure is a simple superposition of crystals *a* and *b* data. The same can be also concluded as to the reflection map in the case of two distant 2D PhCr islands, when optical contact can be considered as negligible. Shown in Figs. 3a and 3b are the spectra of standing *p*-polarized waves inside the coinciding TIR region of isolated glass-glass and glass-

air finite photonic structures. The vertical panel limited here by the glass-1 angle $\theta_1 = 54^\circ$ demonstrates a simple superposition of two spectra for the far away one from another crystals. The high-contrast glass-1-air structure has narrow bands and wide gaps quite opposite to the low-contrast structure fabricated from two kinds of glass.

The integrated circuits based on assemblies of photonic crystal resonators may serve for aids of all-optical signal processing. Therefore, the interaction of close located resonators is of great interest for optimal design of all-optical logic devices.

3. The opto-pneumatic medium as a multiscale pressure indicator

The pneumatic photonic crystals can exhibit significant optical sensitivity to variations of the external pressure and/or temperature [21, 22]. It was shown there that a gas containing 1D elastic PhCr may be used as an optical indicator with several measuring scales, which may be organized on the same substrate due to the well expressed identity of the bandgap structure behaviour. Here, we study the possibility to apply the pneumo-optical effects arising in a strip pneumatic photonic crystal to precise measurements of pressure inside a pipe with fluid flow. The system under consideration is shown in Fig. 4. It is a 1D strip photonic crystal consisting of one substrate made long thin layers of a transparent elastic material of width d_1 separated by air voids (d_2), which can vary the lattice period under the action of the external pressure. The light beam reflects at the incident angle θ_1 from the resonator center in the longitudinal normal plane. The strip length is L and strip half-widths are R_A and R_B , for the PhCr's A and B, correspondingly. We assume that for the photonic crystals under consideration all the strip widths $2R$ are much less than the strip length L and, at the same time, the laser beam cross-section size is considered to be much less than the strip widths. Therefore, we can neglect the non-planarity of surfaces in the area of light beam incidence. Also, the strip design allows the beam inclined incidence in the longitudinal normal plane.

In Fig. 4, a general schematic of a 2-scale pressure indicator based on a layered OPM is shown. The stack of plates contains two strip pneumatic photonic crystals A and B, which embraces two scales of pressure indication covering several orders of magnitude. The access to the atmosphere is controlled using the switches 1 and 2. Geometry of light beam incidence is shown for the strip A. The plate deflection ξ , being directed along the vertical z -axis, is a function of the plate coordinates (x, y) . In a general case, the equation for ξ was studied in [23]

$$D\Delta^2\xi = \delta P, \tag{1}$$

where the stiffness parameter of the plate $D = Ed_1^3 / (12(1 - \sigma^2))$, E is the Young modulus, and σ – Poisson's ratio, δP – pressure difference. For our

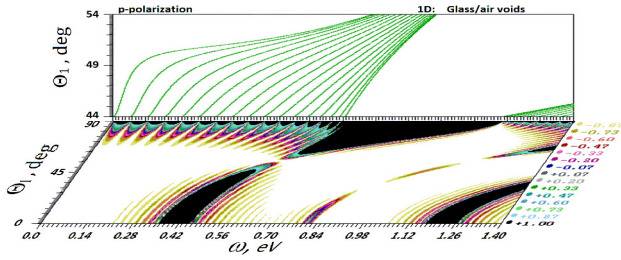


Fig. 5. Vertical panel: the bandgap structure of pneumatic glass/air 1D PhCr inside the TIR region at the propagation angles θ_i in glass from 44° to 54° . $N = 16$, $d_1 = 2 \mu\text{m}$, $d_2 = 2 \mu\text{m}$, photon energy up to 1.4 eV . **Horizontal panel:** color diagram for reflection R of the external incident beam at external (air medium) incident angles θ_i from 0° to 90° . Right column: color scale for reflection coefficient R .

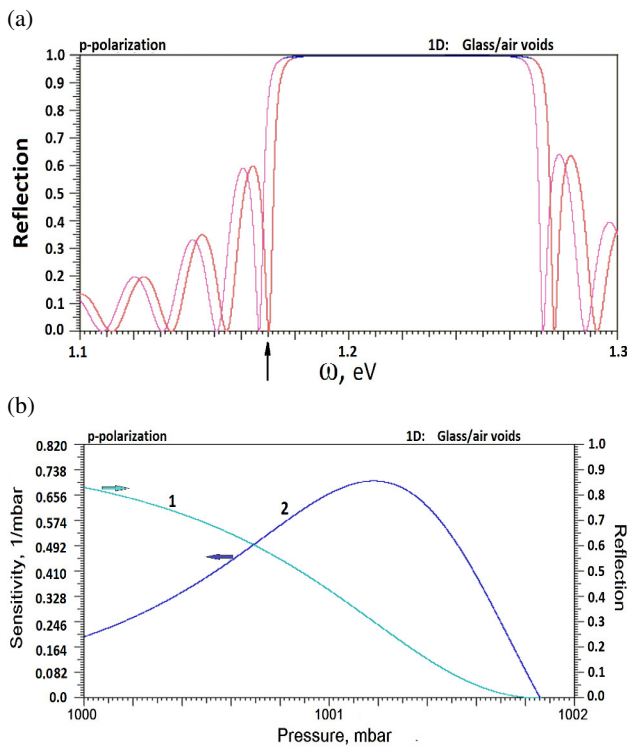


Fig. 6. (a) Quasi-normal incidence ($\theta_i = 1^\circ$) reflection vs photon energy. The two-sided measurement. 15-period glass/air 1D PhCr. $d_1 = 0.5 \mu\text{m}$, $d_2 = 0.8 \mu\text{m}$. Energy gap ($R \approx 1$) is distinguished by color; arrow shows the chosen operating energy $\omega = 1.17 \text{ eV}$. **(b)** Reflection sensitivity vs pressure. Quasi-normal incidence, fixed photon energy $\omega = 1.17 \text{ eV}$ (arrow). 1 – reflection vs pressure dependence (right axis), 2 – sensitivity vs pressure dependence (left axis).

mathematically 1D case, the Laplace operator is written as d^2/dx^2 and, following [23], one can find the solution of (1) satisfying the edge boundary conditions for a fixed long separate elastic strip membranes [21, 22].

A stack of N optically transparent thin plates separated by closed air voids is a system, which optical properties depend on the external pressure and temperature. Initially, the pressure inside the system coincides with the external pressure, and for the above

mentioned geometry of incidence we have a 1D photonic crystal with the period $d_0 = d_1 + d_2$ and the corresponding reflection coefficient $R(P_0)$, where P_0 is the external pressure. The increase of external pressure causes the compression and a decrease in the thickness of air layers d_2 , which changes, in turn, the total reflection pattern. Combining pressures and volumes in neighbouring air voids separated by elastic plates, one can come to the chain of equations

$$P_i = \frac{QP_{00}}{Q - P_{i-1} + 2P_i - P_{i+1}}, \quad i = 1, 2, 3, \dots, N, \quad (2)$$

where $Q = 45Dd_2/R^4$ is the effective elastic pressure of a plate, P_{00} is the initial pressure of the device calibration. It is worth noting that boundary conditions of the system (2) may be chosen as $P_{N+1} = P_0$ in the case of two-sided access of external pressure to the PhCr and $P_{N+1} = P_{00}$. In the limit when the number of plates is sufficiently large, the system (2) describes a continuous *pneumatic medium* [21, 22] with distributed air pressure inside and corresponding deformation of the PhCr. In Fig. 4, a scheme of the one-sided measurement of pressure in a fluid-filled pipe is shown where the PhCr body should be placed into a closed chamber penetrating through the pipe membrane to perform the measurement in a biofluid. The strip A device represents a scale of the first level embracing interval $(10, 10^4)$ mbar, whereas the scale B serves to measure more fine-tuned dynamical changes. Another scheme of measurements – the two-sided one – supposes a free access of the measured pressure to the upper chamber 2 and possesses higher sensitivity in comparison with the one-sided one. Both the bandgap structure and reflection map of the OPM are strongly dependent on the external pressure in two variants of measurements – one-sided (Fig. 4) and two-sided ones. Taking into account the chain of correlations (2), we have calculated the pressure influence on the EMF interaction with a deformed photonic crystal. With the pressure growth, the bands are destroyed and local states arise. In Fig. 6a, the calculated reflection at quasi-normal incidence is plotted within the energy interval $1.1 \dots 1.3 \text{ eV}$ for a 15-period glass/air OPM with the parameters $d_1 = 0.5 \mu\text{m}$ and $d_2 = 0.8 \mu\text{m}$ at quasi-normal angle of incidence $\theta_i = 1^\circ$. In this case, the reflection window (frequency gap) is observed in the energy interval $1.17 \dots 1.27 \text{ eV}$. Due to elasticity of the pneumatic PhCr, any change of the external pressure is accompanied with a shift of the frequency gap. One of the gap sides can be used as the working frequency. We choose the low energy edge of the gap with $\omega = 1.17 \text{ eV}$ (Fig. 6a, arrow). In Fig. 6b, we calculate reflection measured using the device B at the chosen photon energy $\omega = 1.17 \text{ eV}$ for the pressure interval $1000 \dots 1002 \text{ mbar}$, where the reflection coefficient decreases from 0.83 to zero (curve 1). The isothermal sensitivity $\eta = (d\rho/dP)_T$ changes from zero at $P = 1001.86 \text{ mbar}$ to the maximal magnitude 0.698 mbar^{-1} at $P = 1001.18 \text{ mbar}$. In [25], we have discussed the possibilities of a gas containing elastic photonic structure to serve as a sensitive optical

indicator that can unite several pressure scales of accuracy. The indicator includes a layered elastic platform, optical fibers and switching valves, all enclosed into a chamber. At the chosen parameters, the device may cover the pressure interval (0, 10) bar with extremely high accuracy (1 μ bar) for actual pressure values typical for existing inside the biofluid systems of biological organisms. The size of the indicator is close to 1 mm and may be decreased. The miniaturized optical devices considered above may offer an opportunity to organize simultaneous and total scanning monitoring of the biofluid pressure in different parts of the circulatory systems.

4. Pneumatic photonic crystal in metrology

We propose a procedure of high accuracy measurement of pressure based on extra high accuracy volume determination counting in ten significant digits and precise processing the reflected/transmitted optical beam. The improvement procedure for the accuracy of the molar gas constant R from existing eight digits to ten is based on the described above 10^{-10} relative uncertainty of volume and pressure measurement. To obtain the above mentioned accuracy of the universal gaseous constant $R^{(10)}$, one should use an equation of state (both in pneumatic PhCr and surrounding medium) containing the parameters and constants at least of the same accuracy. The Van-der-Waals equation of state takes a view in this case:

$$\left(P + \frac{a^{(10)} v^2}{V^2} \right) \left(\frac{V}{v^{(10)}} - b^{(10)} \right) = R^{(10)} T_{tr}. \quad (3)$$

The problem of inconsistency between the existing relatively low accuracy of parameters like a , b and others as well as the needed output accuracy in 10 significant digits for R is solved using sequential relation of different measurement scales – echeloning. The principle of scale echeloning for precise measurements considered in [21, 22] is based on uniting several sequentially improving accuracy scales in a prolonged measurement. It is important that in the process of echeloning every next stage of measurements is accomplished in absolute uncertainty area of previous one. The situation with improving the accuracy for fundamental constants is to some extent similar to the famous effect of deceleration of Pioneers [24], which needed to take into account a bundle of various undistinguished but nevertheless influential factors beginning with mechanical and heat up to the radiometric ones. Besides, in our case some additional obstacles arise. They are caused by correlation between accuracies of constants, participating parameters, chosen type of the gas state equation, other factors and, finally, measurement procedure. Actually, the experimental procedure of improving the accuracy above the average number of significant digits of parameters is interrelated and recursive. It means that increasing the fundamental constant accuracy is performed by a circle of repeating measurements instantly decreasing relative

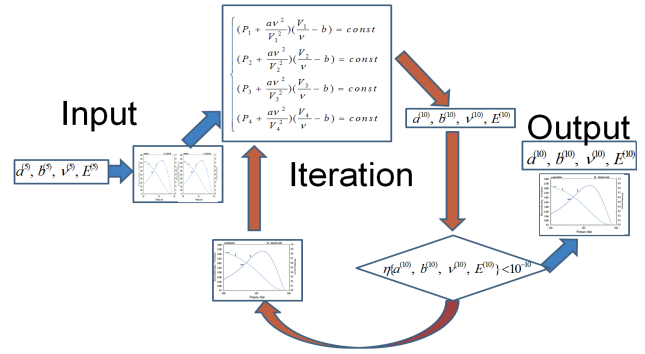


Fig. 7. Scheme of self-consistent procedure improving the accuracy of the parameters a , b , v , E .

uncertainty of the measured constant and parameters (like a and b in Eq. (3)) to the limit uncertainty dictated by accuracy of volume and pressure detection.

In the framework of major level scale of pressure, we have obtained all 200 calibration curves with the set of parameters determined with accuracy not lower than five significant digits, *i.e.*, $a^{(5)}$, $b^{(5)}$, $v^{(5)}$, $E^{(5)}$, $R_l^{(5)}$. This approximately corresponds to relative uncertainty for them 10^{-5} , whereas the volume measuring scale gives the relative uncertainty near 10^{-10} . Therefore, the calibration of the major 0 to 10 bar scale needs some additional after process adjusting, which will be described below as part of this section. In the process of continual measuring the reflection, gas intake is performed from the reservoir to the measuring tube up to the moment when it reaches the known value P_{right} , that corresponds to pressure $P_{min} = 10^{-5} \cdot P_{max} = 10$ Pa and the minimal division of major scale may be marked. With further gas intake the conventional major scale of pressure is filled by divisions in correspondence with the obtained calibration curves up to the limit value 10 bar (Fig. 7, Input). In our case, this procedure is considered as carried out on default. The gas temperature is taken equal to the triple point of water $T_{tr} = 273.16$ K.

In the framework of junior level of pressure by using the calibrated B detector (Fig. 4) in the process of fine increasing the pressure in every interval of 0.1 Pa beginning with zero pressure. For our goal, this interval can be chosen in the vicinity of several reference pressures. In Fig. 7, a scheme of accuracy improving for all the measurement system at reference pressures and volumes (P_1, V_1) , (P_2, V_2) , (P_3, V_3) and (P_4, V_4) is shown. A significant calibration problem is a discrepancy between the needed accuracy of junior scale and low accuracy of parameters at initial stage. Therefore, the scale calibration curves are corrected in a self-consistent procedure step by step with correcting in 6th–10th significant digits of parameters. The entry into the procedure is performed with a set of 5-digit parameters $a^{(5)}$, $b^{(5)}$, $v^{(5)}$, $E^{(5)}$ (Fig. 7, left part). The first calibration curve (Fig. 6b) is used at the input stage with several 10-digit reference points taken from the first interval of pressures (0, 1) μ bar. Solving the system of four equations (upper part of Fig. 7), we find the parameters

a , b , v in their preliminary 10-digit view that in turn adds five significant digits more to the Young modulus E and also leads to modification of the junior level first calibration curve. The latter calls a pressure shift in 6th–10th significant digits, which demands next corrections in the parameters a , b , v , E and so on (Fig. 7, circular arrows). The iteration procedure stops when deviation in the set of parameters became less than 10^{-10} (Fig. 7, right side). At the outlet of the procedure, we correct the parameters $a^{(10)}$, $b^{(10)}$, $v^{(10)}$, $E^{(10)}$, first calibration curve Fig. 5b and first thousand divisions of the total scale. Then the procedure Input-Iteration-Output is repeated for the next one from a hundred calibration intervals of the junior scale. All the junior scale represents the minimal division of major level scale (0, 100) μbar determined now with ten significant digit accuracy. After the corresponding correction of the first calibration curve of major scale, we begin the following hundred step calibration process for the next division of major level scale (100, 200) μbar using the 5-digit calibration curve obtained before as the input data. The latter interval (9.99, 10.00) bar finishes the 10-digit accuracy calibration process.

The iteration procedure serves to determine a group of interrelated physical values with a higher accuracy, *i.e.*, the pressure phenomenon (I) is measured through the phenomenon of pressure caused membrane deformation inside a gas-filled opto-photonic medium (II) and the phenomenon of reflection modification (III) with the corresponding optical signal transformation and processing (IV). We consider that the stages III and IV already have the needed accuracy of their opto-electronic scales but taking into account that initial calibration of the detector was based on inaccurate digits beginning with 6th and up to 10th (Young modulus, for instance), then the measurement procedure should be built on the 10 digit reference points (P_3 , V_3) with consecutive improving the parameters to the needed 10-digit accuracy.

It worth to note that the discussed iteration method is irrelevant to the physical type of pressure gauges used: thermodynamical, electrical, magnetic, *etc.* Iterations are applicable if the procedure converges to (a) an unique constant value in the limits of needed significant digits and (b) this value is the correct one. An important argument in favor of efficiency of iteration procedure in our case is extremely narrow area of pressure and volume dispersion at the final stage of calibration: values P_i and V_i in the central part of Fig. 7 differ one from another only beginning with 6th significant digit. Therefore, the described equations (2) and (3) may be considered as an almost flat surface in a 5-dimensional space of parameters a , b , v , E , R having unique solution that can be found in the process of iterations.

It worth noting that the number of significant digits has an immediate relation to relative uncertainty only for direct measurement of gas volume in our setup. The relative uncertainty of pressure and other physical quantities can be determined in the standard series of measurements under given conditions.

5. Conclusions

Recent progress in nonlinear material science and technology put in the forefront the photonic crystals, perspective optical materials, which can serve as reflecting media surrounding optical waveguides and active resonator structures processing the signal amplitude, phase and polarization. Various kinds of nonlinear effects and approaches are discussed regarding to signal processing and sensing in photonic structures. A novel photonic crystal type, island resonator, was investigated analytically and numerically, and the photonic bandgap structure, field distribution and classification concept of resonator's modes have been proposed. The discussed above PhCr islands are perspective objects for all-optical processing domain, which can be used as elements of logic gates and adder architecture.

One more topic, gas-containing pneumatic photonic crystal, was considered as an optical indicator of pressure uniting several pressure scales of magnitude. The indicator includes layered elastic platform, optical fibers and switching valves. The devices considered may offer an opportunity to organize simultaneous and total scanning monitoring of biofluid pressure in different parts of the circulatory system.

A procedure based on extra-accurate volume controlling and high sensitive pressure measurements was proposed to determine the universal molar gas constant R with approximately 10 significant digits accuracy. With this aim, a two-scale pneumatic photonic crystal is used for precise optical indication of pressure. A self-consistent iteration procedure increasing initial accuracy of parameters and the molar gas constant to the level of volume and pressure accuracy measurements has been studied.

References

1. Dongarra J.J. *Performance of Various Computers Using Standard Linear Equations Software*. Oak Ridge National Laboratory. 2014. P. 1–110. <http://netlib.org/benchmark/performance.pdf>.
2. Rayleigh J.W.S. On the maintenance of vibrations by forces of double frequency and on the propagation of waves through a medium endowed with a periodic structure. *Phil. Mag.* 1887. **24**(147). P. 145–159. <https://doi.org/10.1080/14786448708628074>.
3. Yablonovitch E. Inhibited spontaneous emission in solid-state physics and electronics. *Phys. Rev. Lett.* 1987. **58**, No 20. P. 2059–2062. <https://doi.org/10.1103/PhysRevLett.58.2059>.
4. John S. Strong localization of photons in certain disordered dielectric superlattices. *Phys. Rev. Lett.* 1987. **58**, No 23. P. 2486–2489. <https://doi.org/10.1103/PhysRevLett.58.2486>.
5. Werber A., Zappe H. Tunable, membrane-based, pneumatic micro-mirrors. *J. Opt. A: Pure Appl. Opt.* 2006. **8**. P. 313–317. <https://doi.org/10.1109/OMEMS.2005.1540115>.

6. Pervak V., Ahmad I., Trubetskov M.K., Tikhonravov A.V., Krausz F. Double-angle multilayer mirrors with smooth dispersion characteristics. *Opt. Exp.* 2009. **17**, No 10. P. 7943–7951. <https://doi.org/10.1364/OE.17.007943>.
7. Tokranova N., Xu B., Castracane J. Fabrication of flexible one-dimensional porous silicon photonic band-gap structures. *MRS Proc.* 2004. **797**. <https://doi.org/10.1557/PROC-797-W1.3>.
8. Grzybowski B., Qin D., Haag R., Whitesides G.M. Elastomeric optical elements with deformable surface topographies: applications to force measurements, tunable light transmission and light focusing. *Sensors and Actuators*. 2000. **86**, No 1–2. P. 81–85. [https://doi.org/10.1016/S0924-4247\(00\)00421-0](https://doi.org/10.1016/S0924-4247(00)00421-0).
9. Ouellette J. Seeing the future in photonic crystals. *The Industrial Physicist*. 2002. **7**, No 6. P. 14–17.
10. Sakoda K. *Optical Properties of Photonic Crystals*. Berlin. Springer Verlag, 2001.
11. Winn N.Y., Fink S., Fan Y., and Joannopoulos J.D. Omnidirectional reflection from a one-dimensional photonic crystal. *Opt. Lett.* 1998. **23**. P. 1573–1575. <https://doi.org/10.1364/OL.23.001573>.
12. Deopura M., Ullal C.K., Temelkuran B., and Fink Y. Dielectric omnidirectional visible reflector. *Opt. Lett.* 2001. **26**. P. 1197–1199. <https://doi.org/10.1364/OL.26.001197>.
13. Loncar M., Doll T., Vuchkovich J., Scherer A. Design and fabrication of silicon photonic crystal optical waveguides. *J. Lightwave Technol.* 2000. **18**. P. 1402. <http://resolver.caltech.edu/CaltechAUTHORS:LONjlt00>.
14. Loncar M., Nedeljkovic D., Doll T., Vuckovic J., Scherer A., and Pearsall T.P. Waveguiding in planar photonic crystals. *Appl. Phys. Lett.* 2000. **77**, No 13. P. 1937–1939. <https://doi.org/10.1063/1.1311604>.
15. Kawai N., Inoue K., Carlsson N., Ikeda N., Sugimoto Y., Asakawa K., Takemori T. Confined band gap in an air-bridge type of two-dimensional AlGaAs photonic crystal. *Phys. Rev. Lett.* 2001. **86**. P. 2289–2292. <https://doi.org/10.1103/PhysRevLett.86.2289>.
16. Shi J., Juluri B.K., Lin S.C.S., Lu M., Gao T., Huang T.J. Photonic crystal composites-based wide-band optical collimator. *J. Appl. Phys.* 2010. **108**. P. 043514 (6 p.). <https://doi.org/10.1063/1.3468242>.
17. Patent WO № 2007094845, USA. All-optical logic gates using nonlinear elements – A1, Aug 23 2007, COVEYTECH LLC (US).
18. Rani P., Kalra Y., Sinha R.K. Design of photonic crystal architecture for optical logic AND gates. *Proc. SPIE*. 2013. **8847**, Photonic Fiber and Crystal Devices: Advances in Materials and Innovations in Device Applications VII. P. 88470X. <https://doi.org/10.1117/12.2023855>.
19. Glushko E.Ya. All-optical signal processing in photonic structures with nonlinearity. *Opt. Commun.* 2005. **247**. P. 275–280. <https://doi.org/10.1016/j.optcom.2004.11.096>.
20. Glushko E.Ya. Island kind 2D photonic crystal resonator. *Ukr. Phys. J.* 2017. **62**, No 11. P. 939–946.
21. Glushko E.Ya. Pneumatic photonic crystals. *Opt. Exp.* 2010. **18**, No 3. P. 3071–3078. <https://doi.org/10.1364/OE.18.003071>.
22. Glushko E.Ya. The conception of scales echeloning for precise optical indication of pressure and temperature. *11th Intern. Conf. on Laser and Fiber-Optical Networks Modeling (LFNM)*, 2011. P. 1–3. <https://doi.org/10.1109/LFNM.2011.6144974>.
23. Landau L.D., Lifshitz E.M. *Theory of Elasticity*. New York, Pergamon Press, 1970.
24. Turyshev S.G., Toth V.T. The Pioneer Anomaly. *Living Rev. Relativity*. 2010. **13**. P. 4–175. <https://doi.org/10.12942/lrr-2010-4>.
25. Glushko E.Ya., Stepanyuk A.N. A pneumatic photonic structure and precise optical indication of pressure over time inside the fluid flow. *Int. J. Biosen. & Bioelectron.* 2018. **4**, No 3. P. 99–102. <http://elibrary.kdpu.edu.ua/xmlui/handle/123456789/2896>.

Authors and CV



E.Ya. Glushko, Professor, Doctor of Sciences, Lead Scientific Researcher of Laboratory for semiconductor photonic structures at the V. Lashkaryov Institute of Semiconductor Physics. The area of his scientific interests includes physical optics; photonic crystals; nonlinear phenomena in

optical materials, all-optical signal processing; optical computing and logical gates; mirror-type meta-structures; channel projecting optics; electron and phonon transport in nanostructures and quantum molecular bridges; mechanical engineering and liquid based protecting systems.



A.N. Stepanyuk, born in 1982. University lecturer, Kryvyi Rih State Pedagogical University. The area of his scientific interests includes photonic structures as perspective constructional materials for novel types of all-optical sensors and logical gates.